Received May 24, 2019, accepted June 22, 2019, date of publication June 28, 2019, date of current version July 23, 2019.

Digital Object Identifier 10.1109/ACCESS.2019.2925564

A New Structure of High Voltage Gain SEPIC Converter for Renewable Energy Applications

PANDAV KIRAN MAROTI[1], (Member, IEEE), SANJEEVIKUMAR PADMANABAN[2], (Senior Member, IEEE), JENS BO HOLM-NIELSEN[2], MAHAJAN SAGAR BHASKAR[1], (Member, IEEE), MOHAMMAD MERAJ[1], (Student Member, IEEE), AND ATIF IQBAL[1], (Senior Member, IEEE)

[1]Department of Electrical Engineering, Qatar University, Doha, Qatar
[2]Center for Bioenergy and Green Engineering, Department of Energy Technology, Aalborg University, 6700 Esbjerg, Denmark

Corresponding author: Atif Iqbal (atif.iqbal@qu.edu.qa)

This work was supported by the National Priorities Research Program (NPRP) through the Qatar National Research Fund (a member of the Qatar Foundation) under Grant X-033-2-007.

ABSTRACT The paper proposes a new structure of SEPIC with high voltage gain for renewable energy applications. The proposed circuit is designed by amalgamating the conventional SEPIC with a boosting module. Therefore, the converter benefits from various advantages that the SEPIC converter has, such as continuous input current. Also, high voltage gain and input current continuity make the presented converter suitable for renewable energy sources. The modified SEPIC converter (MSC) provides higher voltage gain compared to the conventional SEPIC and recently addressed converters with a single-controlled switch. The analysis of voltage gain in continuous current mode (CCM) and discontinuous current mode (DCM) is analyzed by considering the non-idealities of the semiconductor devices and passive components. The selection of the semiconductor devices depending on the voltage–current rating is presented along with the designing of reactive components. The numerical simulation and experimental work are carried out, and the obtained results prove the feasibility of the MSC concept and the theoretical analysis.

INDEX TERMS DC-DC converter, energy conversion, high voltage gain, SEPIC, renewable energy.

NOMENCLATURE

S	Active switch
L_X, L_Y and L_Z	Inductors
C_1, C_2 and C_3	Capacitors
D_1, D_2 and D_3	Diodes
V_{in} and V_0	Input and output voltage
V_{C1}, V_{C2} and V_{C3}	Average voltage across capacitor C_1, C_2 and C_3.
V_{LX}, V_{LY} and V_{LZ}	Voltage across inductor L_X, L_Y and L_Z.
k	Duty ratio
$(I_{LX})_{min}$, $(I_{LY})_{min}$ and $(I_{LZ})_{min}$	Minimum peak current through inductor L_X, L_Y and L_Z.
$(I_{LX})_{max}$, $(I_{LY})_{max}$ and $(I_{LZ})_{max}$	Maximum peak current through inductor L_X, L_Y and L_Z.
I_{C1}, I_{C2} and I_{C3}	Average current through capacitor C_1, C_2 and C_3.
I_{D1}, I_{D2} and I_{D3}	Average current of diode D_1, D_2 and D_3.
I_{in}, and I_0	Average input and output current
τ	Normalized inductor time constant
τ_B	Boundary normalized inductor time constant
T_S and f_S	Switching time and switching frequency
P_{in} and P_0	Input and output power
R	Resistive load

The associate editor coordinating the review of this manuscript and approving it for publication was Sing Kiong Nguang.

$(L_X)_{cri}$, $(L_Y)_{cri}$, and$(L_Z)_{cri}$	Critical values of inductor L_X, L_Y and L_Z.
ΔI_{LX}, ΔI_{LY}, and ΔI_{LZ}	Peak to peak ripple currents of inductor L_X, L_Y and L_Z.
ΔV_{C1}, ΔV_{C2}, and ΔV_{C3}	Peak to peak ripple voltage of capacitor C_1, C_2 and C_3.
r_{LX}, r_{LY}, and r_{LZ}	Equivalent series resistance of inductor L_X, L_Y and L_Z.
r_{D1}, r_{D2}, and r_{D3}	ON state resistance of diode D_1, D_2 and D_3.
V_{F1}, V_{F2}, and V_{F3}	Internal forward voltage drop of diode D_1, D_2 and D_3.
r_S	ON state resistance of switch S
ϕ, φ, and γ	Voltage drop contributed by inductor L_X, L_Y and L_Z.
ϑ	Voltage drop across switch S
ζ, ψ, and σ	Voltage drop across the diodes D_1, D_2 and D_3.
η	Efficiency
P^S_{loss}, P^D_{loss}, P^L_{loss} and P^C_{loss}	Power loss across the switch S, diodes, inductors and capacitors.
$P^S_{sw-loss}$, P^S_{c-loss},	Switching and conduction power loss by the switch.
$R_{ds(ON)}$	ON state resistance of switch S
V_{DS} and I_S	Drain to source voltage and current across/through switch S
t_r and t_f	Rising and falling switching time of switch S

I. INTRODUCTION

The utilization of existed fossil fuels is tremendously increased in the last decade, which leads to environmental contaminations and increases the cost of the system [1]. These problems attracts the researcher to work on Renewable Energy Resources (RES) such as Photovoltaic (PV), wind turbine, fuel cells, etc. Among these RES, PV is gaining more attraction and become noticeable as consequence of its various advantages such as eco-friendly, abundant in nature, freely available, etc. However, the voltage generated from the PV modules is comparatively low and depends on the environmental conditions [2]. Therefore, in order to boost the PV voltage, series and parallel combinations of PV panels can be a solution to fulfill the load demand, which results in lower efficiency, high cost and large the size of the system [3], [4]. A high voltage gain DC-DC converter can be a practicable solution to boost the low voltage generated from PV. Fig. 1 shows the general architecture of modern smart DC grid system integrated with PV and fuel cell system. To meet the high voltage demand of DC home, electric vehicle, DC microgrid etc. high voltage gain converter is utilized as intermediate stage. The conventional boost, buck-boost, SEPIC, CUK, etc. can be utilized for high voltage applications at maximum duty ratio, but that decreases the efficiency and affects the functionality of converter [5], [6]. Recently, various high voltage gain DC-DC converters have been proposed with utilization of reactive components in boosting stages [7], [8]. In isolated DC-DC converter, High-Frequency Transformer (HFT) adopted to boost the input voltage by adjusting its turn ratio [9], [10]. Nevertheless, voltage based isolated DC-DC converters have high ripple in the input current and high voltage stress across the secondary side. Moreover, the leakage energy, bulky transformer and multistage power conversion process are the main shortcoming of the isolated converters [11]. Besides that, non-isolated DC-DC converters are the impeccable solution for PV application with high efficiency and compact size. In literature, various voltage-boosting techniques such as cascading of converters e.g. Quadratic Boost Converter (QBC) [12], voltage lift structure [13]–[19] or coupled inductor [20]–[22] have adopted with non-isolated converter to achieve high output voltage.

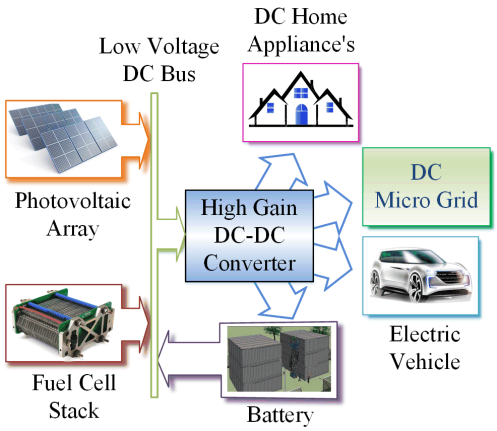

FIGURE 1. Modern smart grid architecture.

In the coupled inductor based converters, the output is controlled by adjusting turns ratio of inductor coil. The leakage inductance of the coupled inductor is inexorable which generates a spike in switch current and demands the clamping

circuit to suppress the current spike [23]. By utilizing the voltage lifting techniques/structures, numerous high gain DC-DC converters have been proposed in [9]–[19]. In [24], second order boost converter with voltage multiplier has been discussed. Presented converter has flexible structure and output voltage depends on the duty ratio as well as on the number of voltage multiplier level. Nonetheless, converter has low voltage gain even though with several numbers of voltage multiplier levels. Additionally, converter has very high input current ripple in the proportion of average input current that implies high-value inductor. In addition, converter has balancing issue of the voltage multiplying capacitors. Moreover, efficiency is decreasing with increasing number of level by the effect of the uncontrolled diodes. A switched capacitor based high gain DC-DC converter with multiple inductors and capacitors has been present in [24]. The presented converter shows the good regulation with lower voltage gain in comparison to the number of components. In [11], high gain switched capacitor DC-DC converter with the active network has been presented. The converter achieves high gain with pulsating current and poor regulation. The converter controlled with two switches and that make the complexity in the control scheme and affects the efficiency. Additionally, discontinues input current is another drawback of the circuitry which proves the minimum utilization of the sources [25].

II. MODIFIED SEPIC CONVERTER

In this paper, a new structure of single switch non-isolated high gain SEPIC is introduced for high voltage application. The MSC has single input-output port and derived by transforming the classical SEPIC as shown in Fig. 2(a). Fig. 2(b) shows the power circuit of MSC consisting three inductors (L_X, L_Y and L_Z), three capacitors (C_1, C_2 and C_3) and three diodes (D_1, D_2 and D_3) which are controlled by single switch S with switching frequency (f_s). In the MSC, inductor L_Y and capacitor C_1 serve as a voltage-boosting element in addition with two diodes. The key features of the proposed MSC are; 1) operates with single switch that reduces the complexity of control circuitry, 2) continuous input current, 3) high voltage gain, 4) maximum utilization of input source.

A. CCM OPERATION AND ANALYSIS

In order to explain the steady state operation, some assumptions are to be consider as: all components to be ideal and all capacitors should be large enough to achieve constant voltage. The MSC controlled by single switch *S,* hence the converter operates in two different modes as mode-I (t_0 to t_1) and mode-II (t_1 to t_2) as shown in Fig. 2(c) and (d) respectively. Where k is duty ratio and $T_S = 1/f_S$ is the time required to complete one switching operation.

1) MODE-I [t_o TO t_1]

In mode-I, three inductors are magnetized with current path as follow: inductor L_X from input supply ($V_{in} - V_{LX} - D_2 - S - V_{in}$), inductor L_Y from capacitor C_1 ($V_{C1} - V_{LY} - S - V_{C1}$) and inductor L_Z from capacitor C_2 ($V_{C2} - S - V_{LZ} - V_{C2}$).

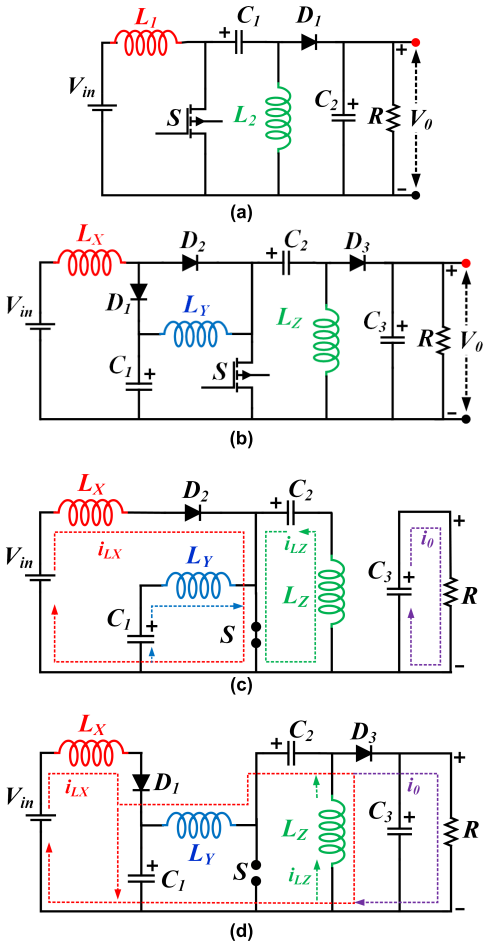

FIGURE 2. Power circuitry of (a) SEPIC and (b) MSC, CCM operating modes of MSC in (c) mode-I and (d) mode-II.

At the same instant, capacitor C_3 reverse bias the diode D_3 and transfer energy to the load as shown in Fig. 2(c). The characteristic waveforms of each component in mode-I are presented in Fig. 3.

$$\left.\begin{aligned} V_{LX} &= V_{in} \\ V_{LY} &= V_{C1} \\ V_{LZ} &= V_{C2} \end{aligned}\right\} \text{mode-I} \tag{1}$$

where, V_{LX}, V_{LY}, V_{LZ} are the voltages across inductor L_X, L_Y, L_Z respectively. V_{C1}, V_{C1} are the voltage across capacitor C_1, C_2 respectively.

2) MODE-II [t_1 TO t_2]

In mode-II, all three inductors are demagnetized as follow: inductor L_X along with input voltage (V_{in}) charges the capacitor C_1 ($V_{in} - V_{LX} - D_1 - C_1 - V_{in}$). The combination of inductor L_Y and capacitor C_1 charges to capacitor C_2 through the path $V_{C1} - V_{LY} - V_{C2} - D_3 - V_0 - V_{C1}$. Also at the same time, inductor L_Z discharges through the load with following the path ($V_{LZ} - D_3 - V_0$) as shown in Fig. 2(d). The characteristic waveforms of each component in mode-II

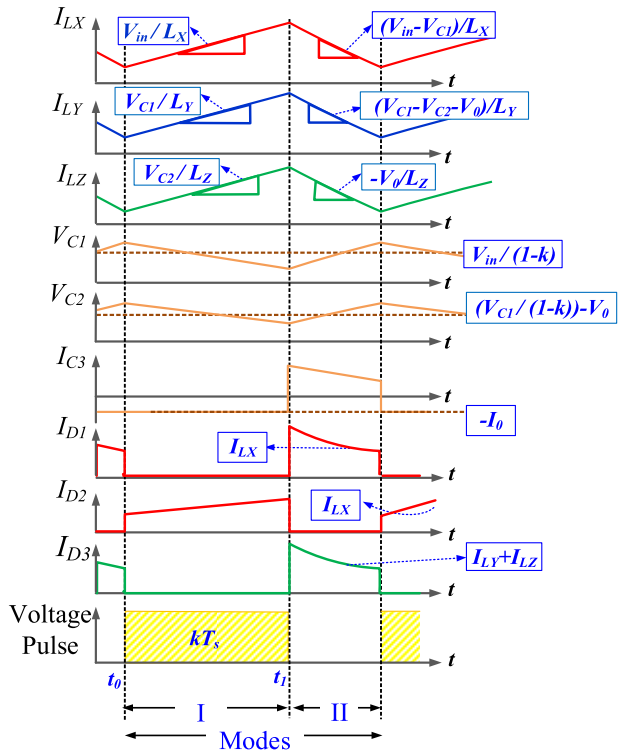

FIGURE 3. Characteristic waveforms of MSC in CCM.

are presented in Fig. 3

$$\left.\begin{aligned} V_{LX} &= V_{in} - V_{C1} \\ V_{LY} &= V_{in} - V_{L1} - V_{C2} - V_0 \\ V_{LY} &= V_{C1} - V_{C2} - V_0 \\ V_{LZ} &= V_0 \end{aligned}\right\} \text{mode-II} \qquad (2)$$

where, V_{C0} is the voltage across capacitor C_3. By applying Inductor Volt Second Balance (IVSB) principle for the inductors L_X, L_Y and L_Z,

$$\frac{V_{C1}}{V_{in}} = \frac{1}{1-k} \qquad (3)$$

$$V_{C2} = \frac{V_{C1}}{1-k} - V_0 \qquad (4)$$

$$\frac{V_0}{V_{C1}} = \frac{k}{1-k} \qquad (5)$$

$$M_{CCM} = \frac{V_0}{V_{in}} = \frac{k}{(1-k)^2} \qquad (6)$$

Equation (6) represents the voltage gain of the proposed converter in CCM mode.

B. DCM OPERATION AND ANALYSIS

The MSC can be operates in Discontinuous Conduction Mode (DCM) as current through inductor/s reaches to zero levels individually or together as respective diode become reverse bias. The DCM operation of MSC is divided into three modes as mode-I, II and III. Where, mode-I and II have similar operating principle similar to CCM. Whereas, mode-III is a prolongation of Mode-II. Based on the inductor current and respective diode operating state, the MSC can be work in three different possible DCM mode as mode-A, mode-B and mode-C. In mode-A, inductor L_X current $(I_{LX})_{min}$ individually reach to zero level as diode D_1 becomes reverse bias. In mode-B, diode D_1 is forward bias and Diode D_3 becomes reverse bias due to inductor L_Y and L_Z current $((I_{LY})_{min},(I_{LZ})_{min})$. Similarly in mode-C, both diodes D_1 and D_3 become reverse bias by the effect of current through inductor L_X, L_Y and L_Z. The power circuitry with respective current path in three possible DCM modes are shown in Fig. 4. Based on the three different possible modes, MSC has three different voltage gain in DCM. Hence, for simplicity the MSC is analyzed with mode-B DCM mode. The respective characteristic waveforms of each component are shown in Fig. 5.

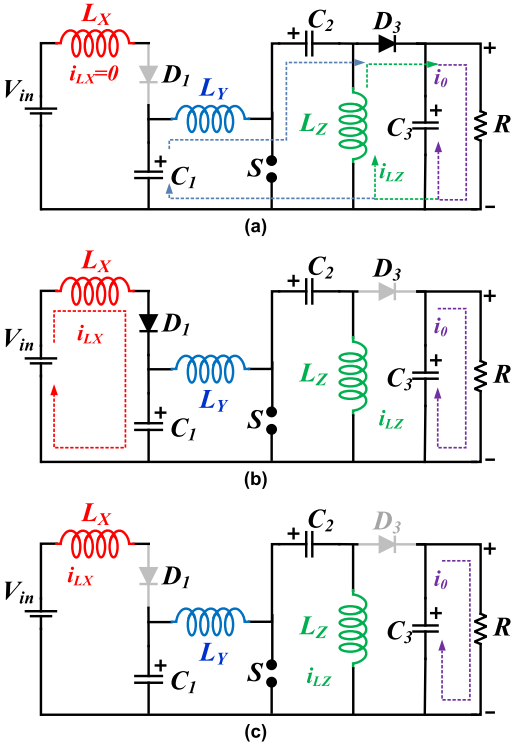

FIGURE 4. Possible DCM operating modes of MSC (a) mode-A, (b) mode-B, and (c) mode-C.

1) MODE-I [t_o TO t_1]

The equivalent circuit is same as mode I of CCM (Fig. 2(c)). In this mode, switches S turned ON. For this mode, the peak amplitude of current through inductor L_X, L_Y and L_Z can be expressed as,

$$\left.\begin{aligned} (I_{LX})_{\max} &= \frac{V_{in}kT_S}{L_X} \\ (I_{LY})_{\max} &= \frac{V_{C1}kT_S}{L_Y} \\ (I_{LZ})_{\max} &= \frac{V_{C2}kT_S}{L_Z} \end{aligned}\right\} \text{mode-I} \qquad (7)$$

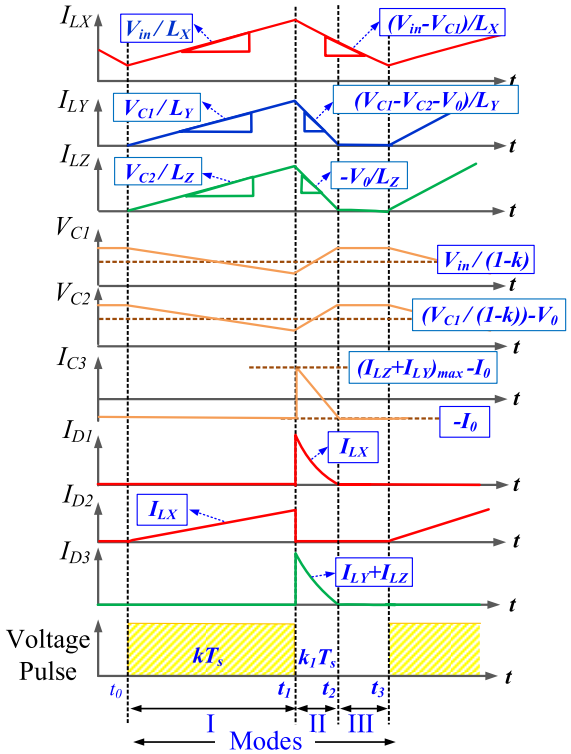

FIGURE 5. Characteristic waveforms of MSC in mode-B of DCM.

2) MODE-II [t_1 TO t_2]

The equivalent circuit is same as mode II of CCM (Fig. 2(d)). In this mode, switches S turned OFF. For this mode, the peak amplitude of current through inductor L_X, L_Y and L_Z can be expressed as,

$$\left.\begin{aligned}(I_{LX})_{\min} &= -\frac{(V_{in}-V_{C1})\,k_1T_S}{L_X}\\ (I_{LY})_{\min} &= -\frac{(V_{C1}-V_{C2}-V_0)\,k_1T_S}{L_Y}\\ (I_{LZ})_{\min} &= \frac{V_0k_1T_S}{L_Z}\end{aligned}\right\}\ \text{mode-II} \qquad (8)$$

3) MODE-III [t_2 TO t_3]

The equivalent circuit of mode-III (mode-B) shown in Fig. 4(b). In this mode, switches S turned OFF. At the end of this mode, the energies stored in inductor L_Y and L_Z are zero. Hence, only energy stored in capacitor C_3 is discharges to the load. Therefore, from (7) and (8),

$$k_1 = \frac{V_{C1}k}{V_0} \qquad (9)$$

From Fig. 5, the average capacitor C_3 current during each switching period is given by

$$\left.\begin{aligned}I_{C3} &= \frac{0.5k_1T_S(I_{LY}+I_{LZ})_{\max}-I_0T_S}{T_S}\\ &= \frac{1}{2}k_1(I_{LY}+I_{LZ})_{\max}-I_0\end{aligned}\right\} \qquad (10)$$

By substituting (7) and (9) in (10), I_{C3} is derived as

$$\frac{V_{C2}k^2T_S}{2}\left(\frac{V_{C2}+V_{C1}}{L}\right) = \frac{V_0}{R} \qquad (11)$$

From (3)-(6), (11) rearranged as

$$M_{DCM} = \frac{V_0}{V_{in}} = \sqrt{\frac{k^2}{(1-k)^2\tau}}, \quad \tau = \frac{L}{RT_S} \qquad (12)$$

where τ is normalized inductor time constant.

Equation (12) represents the voltage gain of the proposed converter in DCM. Using (6) and (12), the boundary for CCM and DCM is derived as

$$\tau_B = (1-k)^2 \qquad (13)$$

where τ_B is boundary normalized inductor time constant.

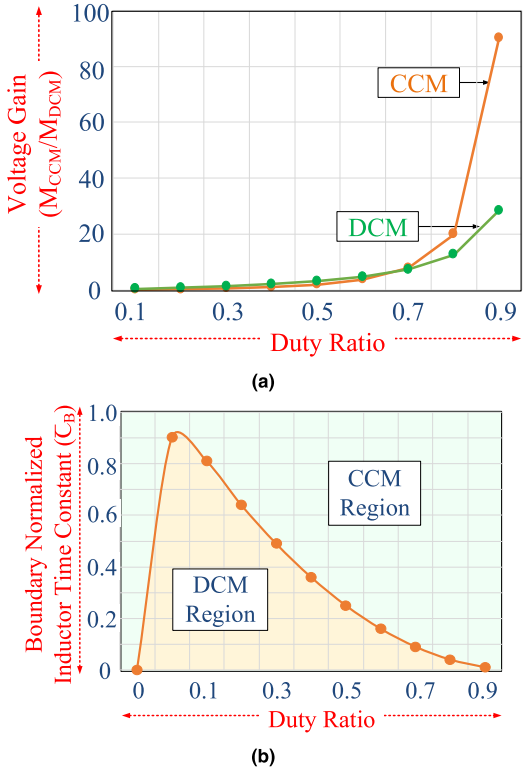

FIGURE 6. (a) Plot of voltage gain of MSC in CCM and DCM Vs. duty ratio and (b) plot of boundary normalized inductor time constant Vs. duty ratio.

The plot of voltage gain of MSC in CCM and DCM mode Vs. duty ratio is depicted in Fig. 6(a). Fig. 6(b) represents the graph of boundary normalized inductor time constant Vs. duty ratio. It is noteworthy that, if τ is greater than τ_B, then MSC operates in CCM. It is investigated that, after attaining the peak value there is decrement in normalized inductor time constant (τ_B) when duty ratio k is increased.

C. DESIGN CONSIDERATION OF INDUCTORS

The selection of inductor is depends on the duty ratio, switching frequency and resistive load [3]. The current carrying

capacity and critical value of respective inductor to operate MSC in CCM is derived by;

$$(V_{LX})_{ON} = \left(L_X \frac{di_{LX}}{dt}\right)_{ON} = V_{in} \tag{14}$$

where I_{LX} is a current flowing through inductor L_X and dt is a change in time. Rearranging (14)

$$\left.\begin{aligned} L_X \frac{\Delta I_{LX}}{kT_S} &= V_{in} \\ \Delta I_{LX} &= \frac{kV_{in}}{f_S L_X} \end{aligned}\right\} \tag{15}$$

where f_S is a switching frequency to control the switch S. To find the input inductor L_X current, equate input power to output power.

$$P_{in} = P_0 = V_{in} I_{LX} = \frac{V_0^2}{R} \tag{16}$$

Rearranging the (16) and equating to (6)

$$I_{LX} = \frac{k^2 V_{in}}{(1-k)^4 R} \tag{17}$$

The maximum and minimum value of inductor current I_{LX} is derived as

$$(I_{LX})_{\max} = I_{LX} + \frac{\Delta I_{LX}}{2} = \frac{k^2 V_{in}}{(1-k)^4 R} + \frac{V_{in} k}{2L_X f_S} \tag{18}$$

$$(I_{LX})_{\min} = I_{LX} - \frac{\Delta I_{LX}}{2} = \frac{k^2 V_{in}}{(1-k)^4 R} - \frac{V_{in} k}{2L_X f_S} \tag{19}$$

To operate the converter in CCM mode, the inductor current must remain positive. To determine the boundary condition between CCM and DCM, $(I_{LX})_{min}$ is set to zero in (19)

$$(L_X)_{crit} = \frac{(1-k)^4 R}{2f_S k} \tag{20}$$

By (20) gives the critical value of inductor L_X below which $(L_X < (L_X)_{crit})$ MSC work in DCM mode and work in CCM as $L_X > (L_X)_{crit}$.

With the same concept, the ripple content of I_{LY} can be derived from (4) as

$$\Delta I_{LY} = \frac{kV_{C1}}{f_S L_Y} = \frac{kV_{in}}{f_S (1-k) L_Y} \tag{21}$$

The MSC has cascaded connection of boost followed by SEPIC converter. As SEPIC receives the input from boost converter, the inductor L_Y current can be derived as,

$$\left.\begin{aligned} V_{C1} I_{LY} &= \frac{V_0^2}{R} \\ I_{LY} &= \frac{V_0^2}{V_{C1} R} = \frac{k^2 V_{in}}{(1-k)^3 R} \end{aligned}\right\} \tag{22}$$

The maximum and minimum peak value of inductor current I_{LY} can be derived as

$$(I_{LY})_{\max} = I_{LY} + \frac{\Delta I_{LY}}{2} = \frac{k^2 V_{in}}{(1-k)^3 R} + \frac{V_{in} k}{2(1-k) L_Y f_S} \tag{23}$$

$$(I_{LY})_{\min} = I_{LY} - \frac{\Delta I_{LY}}{2} = \frac{k^2 V_{in}}{(1-k)^3 R} - \frac{V_{in} k}{2(1-k) L_Y f_S} \tag{24}$$

To determine the boundary condition between CCM and DCM arries by the inductor L_Y current, $(I_{LY})_{min}$ is set to zero in (24)

$$(L_Y)_{crit} = \frac{(1-k)^2 R}{2f_S k} \tag{25}$$

With the same concept, the current ripple of inductor L_Z is derived from (1) and (9) as

$$\Delta I_{LZ} = \frac{kV_{C2}}{f_S L_Z} = \frac{kV_{in}}{f_S (1-k) L_Z} \tag{26}$$

In MSC, the current through inductor L_Z is load current and can be derived as

$$I_{LZ} = \frac{V_0}{R} = \frac{kV_{in}}{(1-k)^2 R} \tag{27}$$

The maximum and minimum value of inductor current (I_{LZ}) are

$$(I_{LZ})_{\max} = I_{LZ} + \frac{\Delta I_{LZ}}{2} = \frac{kV_{in}}{(1-k)^2 R} + \frac{V_{in} k}{2(1-k) L_Z f_S} \tag{28}$$

$$(I_{LZ})_{\min} = I_{LZ} - \frac{\Delta I_{LZ}}{2} = \frac{kV_{in}}{(1-k)^2 R} - \frac{V_{in} k}{2(1-k) L_Z f_S} \tag{29}$$

By equating $(I_{LZ})_{min}$ to zero in (29), The critical value of inductor L_Z can be derived after rearranging as

$$(L_Z)_{crit} = \frac{(1-k)R}{2f_S} \tag{30}$$

D. DESIGN CONSIDERATION OF CAPACITORS

The value of capacitors depends on the voltage ripple (ΔV_{C1} in C_1, ΔV_{C2} in C_2 and ΔV_{C3}in C_3), duty ratio, load resistance, and switching frequency [3]. All three capacitors C_1, C_2 and C_3 are selected with following expression as;

$$\left.\begin{aligned} |\Delta Q| &= \frac{V_{C1}}{R} kT_S = C_1 \Delta V_{C1} \\ \Delta V_{C1} &= \frac{V_{C1} k}{RC_1 f_S} \end{aligned}\right\} \tag{31}$$

The output stage consisting of the diode D_3, capacitor C_3, and the load resistor is the same as in the boost converter, so the output ripple voltage is same as the first stage boost converter and it is express as

$$\Delta V_{C3} = \frac{V_{C3} k}{RC_3 f_S} \tag{32}$$

The voltage variation in capacitor C_2 is determined to from the circuit with the switch closed as presented in Fig. 3. From the definition of capacitance and accounting the magnitude of the charge,

$$\left.\begin{aligned} \Delta V_{C2} &= \frac{\Delta Q_{C2}}{C_2} = \frac{I_0 k T_S}{C_2} \\ &= \frac{V_0 k}{R f_S C_2} \end{aligned}\right\} \tag{33}$$

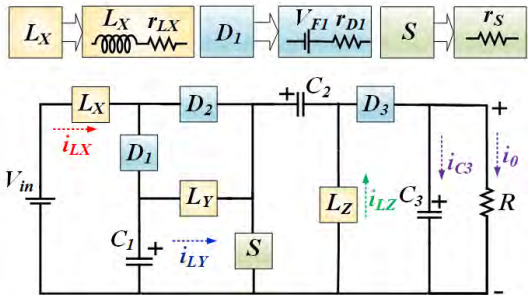

FIGURE 7. MSC with ESR of inductor, switch and voltage drop of diodes.

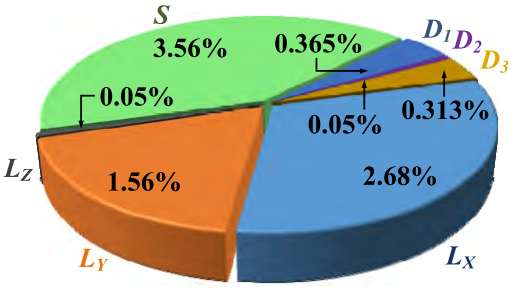

FIGURE 8. Voltage drop across each component with respect to output voltage in (%) at 0.7 duty ratio.

III. EFFICIENCY ANALYSIS AND COMPARISON

A. EFFICIENCY ANALYSIS

In this sub-section, converter efficiency analysis is discussed. The equivalent circuit of MSC with non-idealities of circuit components i.e. internal resistance of respective components is shown in Fig. 7. Where r_{LX}, r_{LY}, r_{LZ} are the Equivalent Series Resistance (ESR) of inductor L_X, L_Y and L_Z respectively. Similarly r_{D1}, r_{D2}, r_{D3} are internal resistance and V_{F1}, V_{F2}, V_{F3} are the forward voltage drop of three diodes D_1, D_2 and D_3 respectively. Whereas, r_S is forward ON state resistance of a controlled switch S.

The equivalent voltage equations of three inductors with consideration of non-idealities in conducting and non-conducting state are

$$\left.\begin{aligned} &V_{LX} = V_{in} - i_{LX}(r_{LX} + r_S + r_{D2}) \\ &-i_{LY}r_S - i_{LZ}r_S - V_{F2} \\ &V_{LY} = V_{C1} - i_{LX}r_S - i_{LY}(r_{LY} + r_S) \\ &-i_{LZ}r_S \\ &V_{LZ} = V_{C2} - i_{LX}r_S - i_{LY}r_S \\ &-i_{LZ}(r_S + r_{LZ}) \end{aligned}\right\} \text{ ON state} \quad (34)$$

$$\left.\begin{aligned} &V_{LX} = V_{in} - i_{LX}(r_{LX} + r_{D1}) \\ &-V_{F1} - V_{C1} \\ &V_{LY} = V_{C1} - i_{LY}(r_{LY} + r_{D3}) \\ &-i_{LZ}r_{D3} - V_{F3} - V_{C2} - V_0 \\ &V_{LZ} = -V_0 - i_{LZ}(r_{LZ} + r_{D3}) \\ &-i_{LY}r_{D3} - V_{F3} \end{aligned}\right\} \text{ OFF state} \quad (35)$$

By the principle of IVSB, the resultant output voltage of MSC in terms of voltage drops across each component can be expressed as;

$$V_0 = \frac{kV_{in}}{(1-k)^2} - \begin{bmatrix} r_{LX}\phi + r_{LY}\varphi + r_{ZD}\gamma \\ +r_S\vartheta + r_{D2}\psi + r_{D1}\zeta + r_{D3}\sigma \end{bmatrix} \quad (36)$$

where,

$\left.\phi = \frac{V_{in}k^3}{R(1-k)^5}\right\}$ voltage drop across inductor L_X,

$\left.\varphi = \frac{V_{in}k^3}{R(1-k)^4}\right\}$ voltage drop across inductor L_Y,

$\left.\gamma = \frac{kV_{in}}{R}\right\}$ voltage drop across inductor L_Z,

$\left.\vartheta = \frac{kV_{in}}{R(1-k)^2}\left(\frac{(2-k)k^2}{(1-k)^2} + k^3(2-k) + 1 + (1-k)^2\right)\right\}$ by switch S,

$\left.\zeta = \frac{kV_{in}}{R(1-k)^2}\left(k^2 + V_{F1}\right)\right\}$ voltage drop across diode D_1,

$\left.\psi = \frac{k^3V_{in}}{R(1-k)^4}\left(k + V_{D2}\right)\right\}$ voltage drop across diode D_2,

$\left.\sigma = \frac{kV_{in}}{R(1-k)^2}\left(1 - k + V_{F3}\right)\right\}$ voltage drop across diode D_3.

The percentage of voltage drop across each inductor, diode and switch by their ESR with respect to output voltage is depicted in Fig. 8. It is observed that, switch S has higher contribution (3.56%) in voltage drop as compared to other circuit components at 0.7 duty ratio. However, diode D_2 and inductor L_Z have relatively less contribution (0.05%) in voltage drop. The voltage gain and efficiency of the converter are affected by conduction loss due to the parasitic resistance of circuit element and switching loss by the semiconductor devices. Equation (37) gives the relation of output power with the efficiency. To evaluate the power losses and efficiency of MS converter, the losses can be calculated as for each component,

$$\eta = \frac{P_0}{P_0 + P_{loss}} = \frac{P_0}{P_0 + P^S_{loss} + P^D_{loss} + P^L_{loss} + P^C_{loss}} \quad (37)$$

where, P^S_{loss} is loss across switches, P^D_{loss} is loss across diodes, P^L_{loss} is loss by inductors, and P^C_{loss} is loss by capacitors. However, the switching and conduction loss of switches can be calculated based on the following equations for each switch.

$$\left.\begin{aligned} P^S_{loss} &= P^S_{c-loss} + P^S_{sw-loss} \\ P^S_{c-loss} &= R_{ds(on)}I^2_S \\ P^S_{sw-loss} &= \frac{1}{2}V_{DS}I_S(t_r + t_f)f_s \end{aligned}\right\} \quad (38)$$

where, P^S_{c-loss} is a conduction loss contributed by switch, $P^S_{sw-loss}$ is a switching loss contributed by switch, $R_{ds(on)}$ is ON-state resistance, V_{DS} is a voltage across switch in OFF state, t_r and t_f are rising and falling time of switch and f_s represents the switching frequency of switch. With the help of (17), (22), (27), and (38) the expression of switching and conduction loss of MS converter is derived

$$\left.\begin{aligned} P^S_{SW-loss} &= \frac{k^2V^2_{in}}{2R(1-k)^4}(t_r + t_f)f_s \\ P^S_{C-loss} &= R_{dS(ON)}\left[\frac{kV_{in}}{R(1-k)^4}\right]^2 \end{aligned}\right\} \quad (39)$$

TABLE 1. Comparison of MSC with existing high gain converters.

Topologies	Number				V_{DS}	M_{CCM}
	L	C	S	D		
[5]	2	3	1	2	$V_0/(1+k)$	$(1+k)/(1-k)$
[6]	4	6	1	3	$V_0/2$	$3k/(1-k)$
[11]	2	3	2	3	$V_0/(2+k)$	$(2+k)/(1-k)$
[16]	1	3	1	3	$V_0/2$	$2/(1-k)$
[20]	1	4	1	4	$V_0/(3-k)$	$(3-k)/(1-k)$
[24]	2	3	2	3	$V_0(1-k)$, kV_0	$1/k(1-k)$
[25]	2	3	1	2	$V_0/2k$	$2k/(1-k)$
[26]	3	3	1	5	V_0/k^2	$k^2/(1-k)^2$
QBC	2	2	1	3	V_0	$1/(1-k)^2$
MSC	3	3	1	3	V_0	$k/(1-k)^2$

L: inductor, C: capacitor, D: diode, S: switch, V_{DS}: voltage across switch, M_{CCM}: voltage gain (V_0/V_{in})

TABLE 2. Simulation and hardware parameters of MS converte.

Parameter	Hardware Prototype
Input Supply	24 V
Switching frequency	50 kHz
Duty ratio	70 %
Power	100 W
Load (Resistive)	350 Ω
Inductors (L_X, L_Y and L_Z)	≈1 mH, 15 A (shell type)
Cap. (C_1, C_2 and C_3)	220 µF, 350 V (electrolyte)
Switch	Power MOSFET (FDP19N40), V_{DS}: 400V, I_D:9 A
Diodes	Power diode (STTH30R04)

The power loss by each diode can be calculated as

$$\left.\begin{aligned} P^D_{loss} &= \left(V_F \times I_{D(avg)}\right) + \left(r_D \times i^2_{D(rms)}\right) \\ &= \frac{V_{in}k(1-k+k^2)}{R(1-k)^4} \end{aligned}\right\} \quad (40)$$

The power loss by the capacitors and inductors can be derived as

$$\left.\begin{aligned} P^C_{loss} &= r_C i^2_{C,rms} \\ P^L_{loss} &= r_L i^2_{L,rms} \end{aligned}\right\} \quad (41)$$

where r_C is ESR of capacitor. In this paper, magnetic loss by inductor and body diode conduction loss in switches are not considered.

B. COMPARISON WITH RECENTLY ADDRESED CONVERTERS

The proposed MSC is compared with recently addressed high gain converters as discussed in the literature. The comparison is made in term of number of active and passive components requirements, voltage stress across controlled switch (V_{DS}), voltage gain (M_{CCM}) as tabulated in Table 1. It is observed that, the MSC required less components as compared to other converters. From Fig. 9, it is noticed, the proposed converter gives higher voltage gain as compared to other converters.

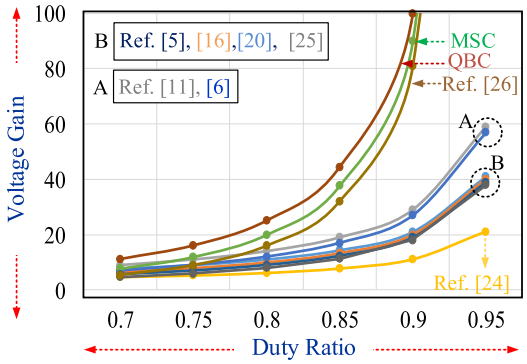

FIGURE 9. Graph of voltage gain of recently addressed converter and MSC Vs duty ratio.

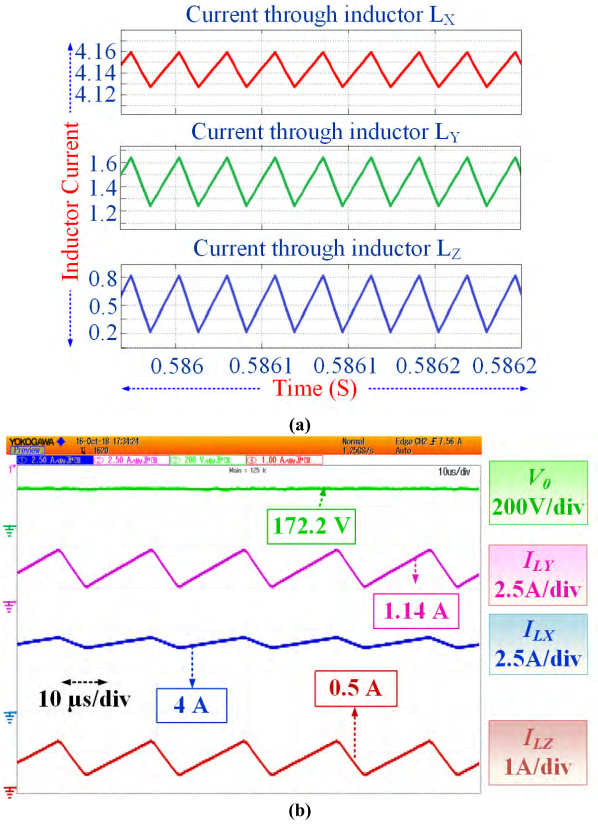

FIGURE 10. Waveform of current through inductor L_X, L_Y and L_Z in (a) simulation and (b) hardware.

IV. DISCUSSION ON SIMULATION AND HARDWARE RESULTS

The simulation and experimental work of proposed converter is performed to test its functionality. The MSC is implemented according to the aforementioned design procedure with the parameters given in Table 2. To operate the converter in CCM, the inductors L_X, L_Y and L_Z values are selected more than respective critical value as derived in (14), (15) and (16), respectively. The gate pulse with 70 % duty ratio is generated through Virtex-5 FPGA. Fig. 10(a) depicts the simulation result waveform of inductor L_X, L_Y and L_Z current.

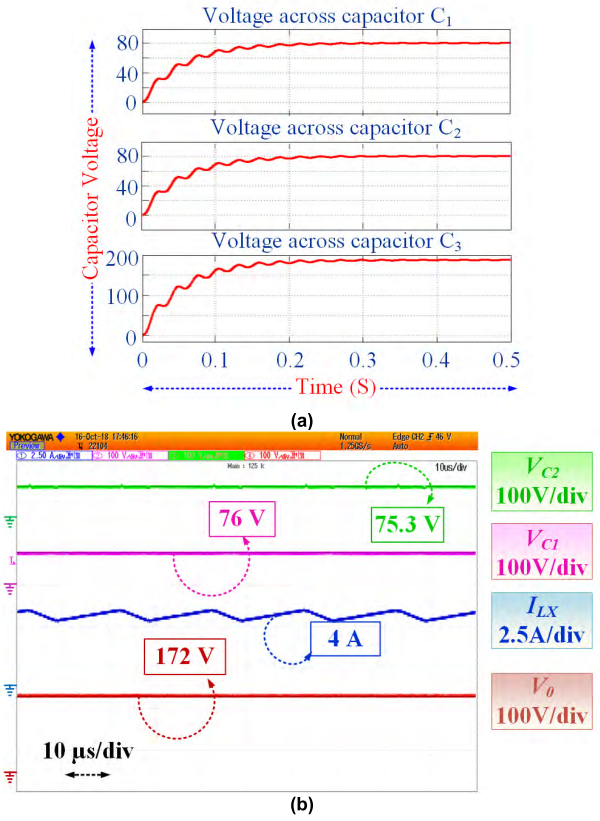

FIGURE 11. Waveform of voltage across capacitor C_1, C_2 and C_3 in (a) simulation and (b) hardware.

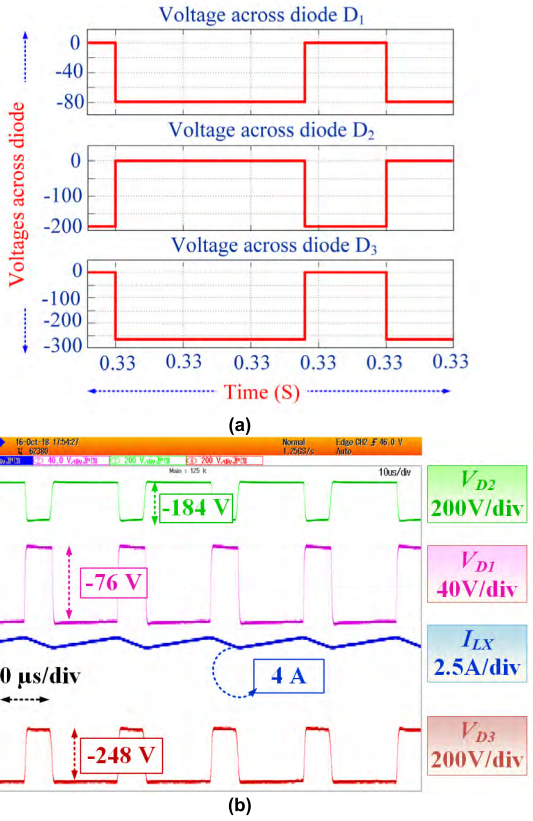

FIGURE 12. Waveform of voltage across diode D_1, D_2 and D_3 in (a) Simulation and (b) hardware.

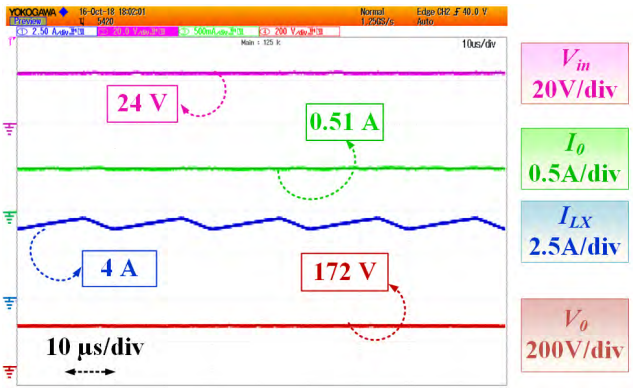

FIGURE 13. Experimental result of input voltage and current; output voltage and current.

It is observed that, inductor L_X, L_Y and L_Z carry 4 A, 1.4 and 0.5 A (average) current. Whereas, Fig. 10(b) shows the experimental result waveform of output voltage (V_0), inductor L_Y current (I_{LY}), L_X (I_{LX}) and L_Z (I_{LZ}) current from top to bottom. During mode-I, current through all three inductors are increasing with positive slope at the same instant. Whereas, in mode-II, it starts decreasing with negative slope as expected. Fig. 11(a) depicts the simulation results waveform of capacitor C_1, C_2 and C_3 voltage. It is observed that, +80 V is developed across the both capacitor C_1 and C_2. Also, non-inverted 186 V across the capacitor C_3.

Fig. 11(b) depicts the experimental waveform of voltage across the capacitor is C_2 and C_1; current through inductor L_X and voltage across capacitor C_3 from top to bottom. A non-inverting 76 V, 75.3 V and 172 V is developed across capacitor C_1, C_2 and C_3 respectively in steady state as observed from Fig. 11(b). Fig. 12(a) and (b) shows the blocking voltage across diode D_1, D_2 and D_3 in reverse bias condition. In mode-I, It is observed that Peak Inverse Voltage (PIV) across diode D_1 is equal to voltage across capacitor C_1 and equal to 76 V. Whereas, PIV across diode D_3 is equal to addition of voltage across capacitor C_2 and C_3 i.e.($V_{C2} + V_0 = 184$V). In mode-II, diode D_2 is reverse bias and handle PIV equal to output voltage (V_0) and equals to 172V. Fig. 13 depicts the hardware result waveform of input voltage (V_{in}), output current (I_0), inductor L_X current (I_{LX}) and output voltage (V_0) from top to bottom. It is noticed from experimental results, MSC operates with 24 V input supply and draw the input current ($I_{LX} = I_{in}$) of 4 A with input power of 96 W. Furthermore, MSC develop 172 V at the load end (V_0) with 0.51 load current (I_0).

The DCM operation of proposed converter depends on the inductors value, duty ratio, value of resistive load and switching frequency. Therefore, the DCM mode can be achieved either by decreasing the duty ratio or switching frequency or by increasing the load resistance value. In this paper, the proposed converter operated in DCM operation by decreasing the duty ratio up to 60 % from 70 % without disturbing the other parameters. The experimental

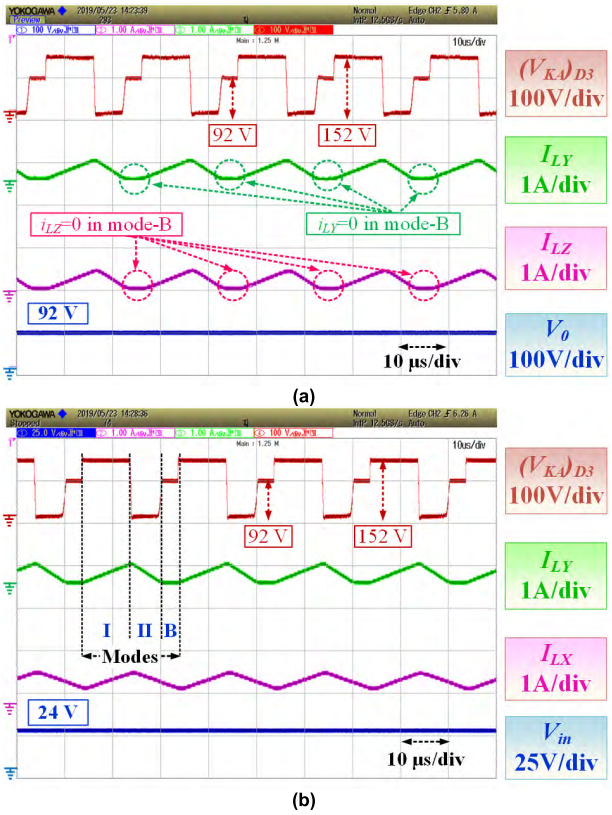

FIGURE 14. Experimental results of proposed converter in DCM mode (a) voltage across diode D_3, inductor L_Y and L_Z current and output voltage and (b) voltage across diode D_3, inductor L_Y and L_X current and input voltage.

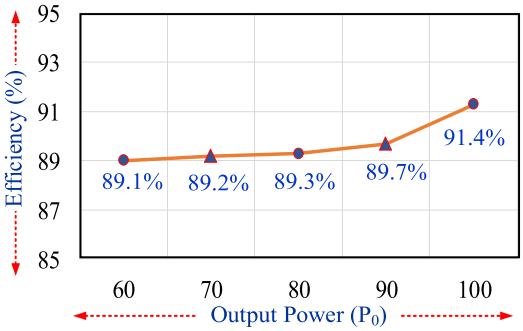

FIGURE 15. Experimental efficiency curve at different power with constant load.

results of proposed converter in DCM mode are shown in Fig. 14. It is observed that, with decrease in duty ratio inductors L_X, L_Y and L_Z current reaches to their maximum level in mode-I. In mode-II, inductors current ($I_{LX} I_{LY}$ and I_{LZ}) start decreasing. Whereas, I_{LY} and I_{LZ} reaches to zero level at the end of mode-II by the effect of reverse bias condition of diode D_3. It worth to note that from experimental results as shown in Fig. 14 (a) and (b), the proposed converter work in DCM mode (mode-B) due to the $I_{LZ} = I_{LY} = 0$. It is observed that, 92 V is developed at the load end at with 24 V input voltage at inductor time $\tau = 0.142$. Whereas, across diode D_3 a 152 V (cathode to anode) voltage is appear as PIV.

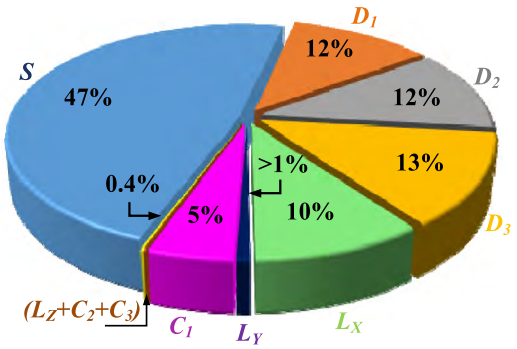

FIGURE 16. Graph of power loss distribution across each component with respect to output power loss in (%) at 0.7 duty ratio.

Efficiency of proposed converter is experimentally analyzed for different power from 60 W to 100 W. It is observed that proposed converter operates with 89.1 % efficiency at 60 W load and 91.4 % at 100 W as shown in Fig. 15. With the help of (37)-(41), the power loss distribution across each component in the proposed converter calculated with ESR as ($r_S = r_L = 0.2\Omega$, $r_C = 0.1\Omega$, $r_D = 0.01\Omega$ and $V_F = 0.9$V). The power loss distribution across the each components is calculated and graphically shown in Fig. 16 with respect to output power loss. It is observed that, the maximum power loss is contributed by switch (47%). Whereas, capacitor C_2, C_3 and inductor L_Z have very less contribution (>1%) in power loss as compared to other components.

V. CONCLUSION

A new structure of high gain modified SEPIC DC-DC converter has been introduced for renewable energy applications. High voltage gain and continuous input current are the advantages of MSC. The working principle of MSC in CCM and DCM mode has been presented. Additionally, the mathematical voltage gain derivation in CCM and DCM mode with non-idealities consideration and parameter design has been shown sequentially. Also, overall comparison between MSC and other non-isolated single switch converters has been addressed. The performance of the proposed converter is tested with numerical simulation and hardware implementation for 100 W prototype model. The results are shown for 172 V output from 24 V input supply with a gain of almost 8. According to the obtained results, it can be concluded that the proposed converter is well suited for high voltage renewable energy applications.

ACKNOWLEDGMENT

The statements made herein are solely the responsibility of the authors. Furthermore, this is to acknowledge that the publication charges of this article was funded by the Qatar National Library, Doha, Qatar.

REFERENCES

[1] F. Blaabjerg, Y. Yang, K. Ma, and X. Wang, "Power electronics—The key technology for renewable energy system integration," in *Proc. Int. Conf. Renew. Energy Res. Appl. (ICRERA)*, Nov. 2015, pp. 1618–1626.

[2] O. Cornea, G.-D. Andreescu, N. Muntean, and D. Hulea, "Bidirectional power flow control in a DC microgrid through a switched-capacitor cell hybrid DC–DC converter," *IEEE Trans. Ind. Electron.*, vol. 64, no. 4, pp. 3012–3022, Apr. 2017.
[3] R. W. Erickson and D. Maksimovic, *Fundamentals of Power Electronics*, 2nd ed. Norwell, MA, USA: Kluwer, 2001.
[4] S. Padmanaban, M. S. Bhaskar, P. K. Maroti, F. Blaabjerg, and V. Fedák, "An original transformer and switched-capacitor (T & SC)-based extension for DC-DC boost converter for high-voltage/low-current renewable energy applications: Hardware implementation of a new T & SC boost converter," *Energies*, vol. 11, no. 4, p. 783, Apr. 2018.
[5] R. Gules, W. M. dos Santos, F. A. F. dos Reis, E. F. R. Romanelli, and A. A. Badin, "A modified SEPIC converter with high static gain for renewable applications," *IEEE Trans. Power Electron.*, vol. 29, no. 11, pp. 5860–5871, Dec. 2014.
[6] M. R. Banaei and S. G. Sani, "Analysis and implementation of a new SEPIC-based single-switch buck–boost DC–DC converter with continuous input current," *IEEE Trans. Power Electron.*, vol. 33, no. 12, pp. 10317–10325, Jan. 2018.
[7] M. Lakshmi and S. Hemamalini, "Nonisolated high gain DC–DC converter for DC microgrids," *IEEE Trans. Ind. Electron.*, vol. 65, no. 2, pp. 1205–1212, Jul. 2018.
[8] W. Li and X. He, "Review of nonisolated high-step-up DC/DC converters in photovoltaic grid-connected applications," *IEEE Trans. Ind. Electron.*, vol. 58, no. 4, pp. 1239–1250, May 2011.
[9] M. Nymand and M. A. E. Andersen, "High-efficiency isolated boost DC–DC converter for high-power low-voltage fuel-cell applications," *IEEE Trans. Ind. Electron.*, vol. 57, no. 2, pp. 505–514, Nov. 2010.
[10] K. I. Hwu and W. Z. Jiang, "Isolated step-up converter based on flyback converter and charge pumps," *IET Power Electron.*, vol. 7, no. 9, pp. 2250–2257, 2014.
[11] Y. Tang, T. Wang, and Y. He, "A switched-capacitor-based active-network converter with high voltage gain," *IEEE Trans. Power Electron.*, vol. 29, no. 6, pp. 2959–2968, Jun. 2014.
[12] M. Nilanjan and S. Dani, "Control of cascaded DC–DC converter-based hybrid battery energy storage systems—Part I: Stability issue," *IEEE Trans. Ind. Electron.*, vol. 63, no. 4, pp. 2340–2349, Dec. 2016.
[13] M. A. Salvador, T. B. Lazzarin, and R. F. Coelho, "High step-up DC–DC converter with active switched-inductor and passive switched-capacitor networks," *IEEE Trans. Ind. Electron.*, vol. 65, no. 7, pp. 5644–5654, Dec. 2018.
[14] A. Alzahrani, M. Ferdowsi, and P. Shamsi, "A family of scalable non-isolated interleaved DC-DC boost converters with voltage multiplier cells," *IEEE Access*, vol. 7, pp. 11707–11721, 2019.
[15] M. S. Bhaskar, M. Meraj, A. Iqbal, S. Padmanaban, P. K. Maroti, and R. Alammari, "High gain transformer-less double-duty-triple-mode DC/DC converter for DC microgrid," *IEEE Access*, vol. 7, pp. 36353–36370, 2019.
[16] B. Wu, S. Li, Y. Liu, and K. M. Smedley, "A new hybrid boosting converter for renewable energy applications," *IEEE Trans. Power Electron.*, vol. 31, no. 2, pp. 1203–1215, Feb. 2016.
[17] D. Gunasekaran, L. Qin, U. Karki, Y. Li, and F. Z. Peng, "A variable (n/m) X switched capacitor DC–DC converter," *IEEE Trans. Power Electron.*, vol. 32, no. 8, pp. 6219–6235, Oct. 2017.
[18] B. P. Baddipadiga and M. Ferdowsi, "A high-voltage-gain DC-DC converter based on modified Dickson charge pump voltage multiplier," *IEEE Trans. Power Electron.*, vol. 32, no. 10, pp. 7707–7715, Oct. 2017.
[19] G. C. Silveira, F. L. Toffoli, L. D. S. Bezerra, and R. P. Torrico-Bascope, "A nonisolated DC–DC boost converter with high voltage gain and balanced output voltage," *IEEE Trans. Ind. Electron.*, vol. 61, no. 12, pp. 6739–6746, Apr. 2014.
[20] Y. Cao, V. Samavatian, K. Kaskani, and H. Eshraghi, "A novel nonisolated ultra-high-voltage-gain DC–DC converter with low voltage stress," *IEEE Trans. Ind. Electron.*, vol. 64, no. 4, pp. 2809–2819, Apr. 2017.
[21] D. Yu, J. Yang, R. Xu, Z. Xia, H.-H. C. Iu, and T. Fernando, "A family of module-integrated high step-up converters with dual coupled inductors," *IEEE Access*, vol. 6, pp. 16256–16266, 2018.
[22] M. Zhang, Y. Xing, H. Wu, H. Hu, and X. Ma, "A dual coupled inductors-based high step-up/step-down bidirectional DC-DC converter for energy storage system," in *Proc. IEEE Appl. Power Electron. Conf. Expo. (APEC)*, Tampa, FL, USA, Mar. 2017, pp. 2958–2963.
[23] G. Wu, X. Ruan, and Z. Ye, "Nonisolated high step-up DC–DC converters adopting switched-capacitor cell," *IEEE Trans. Ind. Electron.*, vol. 62, no. 1, pp. 383–393, May 2015.
[24] J. C. Rosas-Caro, F. Mancilla-David, J. C. Mayo-Maldonado, J. M. Gonzalez-Lopez, H. L. Torres-Espinosa, and J. E. Valdez-Resendiz, "A transformer-less high-gain boost converter with input current ripple cancelation at a selectable duty cycle," *IEEE Trans. Ind. Electron.*, vol. 60, no. 10, pp. 4492–4499, Oct. 2013.
[25] M. R. Banaei, H. Ardi, and A. Farakhor, "Analysis and implementation of a new single-switch buck–boost DC/DC converter," *IET Power Electron.*, vol. 7, no. 7, pp. 1906–1914, 2014.
[26] N. Zhang, G. Zhang, K. W. See, and B. Zhang, "A single-switch quadratic buck–boost converter with continuous input port current and continuous output port current," *IEEE Trans. Power Electron.*, vol. 33, no. 5, pp. 4157–4166, Jun. 2017.

PANDAV KIRAN MAROTI (S'17–M'19) received the bachelor's degree in electronics and telecommunication from Dr. Babasaheb Ambedkar Marathwada University, Aurangabad, India, in 2011, and the M.Tech. degree (Hons.) in power electronics and drives from the Vellore Institute of Technology, Vellore, India, in 2014. He is currently pursuing the Ph.D. degree in power electronics under the guidance of Prof. S. Padmanaban (IEEE Senior Member) and a co-guide Prof. F. Blaabjerg (IEEE Power Electronics President and Fellow) with the University of Johannesburg, South Africa. He was an Assistant Professor with the Marathwada Institute of Technology, Aurangabad, from 2014 to 2016. He is currently a Visiting Researcher with Qatar University. He has published scientific papers in the field of power electronics (multilevel dc/dc and dc/ac converter and multiphase open winding inverter). He is also a Professional Active Member of the Industrial Electronics, Power Electronics, Industrial Application, and the Young Professionals societies. He is also an Active Reviewer Member of various reputed international conferences and journals, including IEEE and IET. He received the Best Paper Award from ETAEERE, in 2016, sponsored Lecture note in Electrical Engineering, Springer book series. He received the Global Experience Scholarship (GES).

SANJEEVIKUMAR PADMANABAN (M'12–SM'15) received the bachelor's degree in electrical engineering from the University of Madras, India, in 2002, the master's degree (Hons.) in electrical engineering from Pondicherry University, India, in 2006, and the Ph.D. degree in electrical engineering from the University of Bologna, Italy, in 2012. He was an Associate Professor with VIT University, from 2012 to 2013. In 2013, he joined the National Institute of Technology, India, as a Faculty Member. In 2014, he was invited as a Visiting Researcher with the Department of Electrical Engineering, Qatar University, Qatar, funded by the Qatar National Research Foundation (Government of Qatar). He continued his research activities at the Dublin Institute of Technology, Ireland, in 2014. He was an Associate Professor with the Department of Electrical and Electronics Engineering, University of Johannesburg, South Africa, from 2016 to 2018. Since 2018, he has been a Faculty Member with the Department of Energy Technology, Aalborg University, Esbjerg, Denmark. He has authored over 300 scientific papers. He is also a Fellow of Institution of Engineers (FIE'18), India, and the Institution of Telecommunication and Electronics Engineers (FIETE'18), India. He received the Best Paper cum Most Excellence Research Paper Award from IET-SEISCON'13 and IET-CEAT'16, and five Best Paper Awards from ETAEERE'16 sponsored Lecture note in Electrical Engineering, Springer book series. He serves as an Editor/Associate Editor/Editorial Board of refereed journals, in particular, the *IEEE Systems Journal*, IEEE Access journals, *IET Power Electronics*, and *Journal of Power Electronics* (South Korea), and the Subject Editor of the *IET Renewable Power Generation*, *IET Generation, Transmission and Distribution*, and *FACTS* journals (Canada).

JENS BO HOLM-NIELSEN is currently with the Department of Energy Technology, Aalborg University, and the Head of the Esbjerg Energy Section. On his research activities, he established the Center for Bioenergy and Green Engineering, in 2009, and serves as the Head of the Research Group. He has vast experience in the field of biorefinery concepts and biogas production—anaerobic digestion. He is also implemented projects of bioenergy systems in Denmark with provinces and European states. He has served as the Technical Advisory for many industries in this field. He has executed many large-scale European Union and United Nation projects in research aspects of bioenergy, bio refinery processes, the full chain of biogas, and green engineering. He has authored more than 300 scientific papers. His focus areas are renewable energy, sustainability, and green jobs for all. He was a member on invitation with various capacities in the committee for over 500 various international conferences and an Organizer of international conferences, workshops, and training programs in Europe, Central Asia, and China.

MAHAJAN SAGAR BHASKAR (M'15) received the bachelor's degree in electronics and telecommunication engineering from the University of Mumbai, Mumbai, India, in 2011, the master's degree in power electronics and drives from the Vellore Institute of Technology, VIT University, India, in 2014, and the Ph.D. degree in power electronics from the Department of Electrical and Electronic Engineering Science, University of Johannesburg, Johannesburg, South Africa, in 2019. He was an Assistant Professor and a Research Coordinator with the Department of Electrical and Electronics Engineering, Marathwada Institute of Technology (MIT), Aurangabad, India. He is currently a Visiting Researcher with the Department of Electrical Engineering, Qatar University, Doha, Qatar. He has published scientific papers in the field of power electronics with particular reference to XY converter family, multilevel dc/dc and dc/ac converter, and high gain converter. He is also a Professional Active Member of *IEEE Industrial Electronics*, *Power Electronics*, *Industrial Application*, *Power and Energy*, *Robotics and Automation*, the Vehicular Technology Societies, the Young Professionals, and various IEEE Councils and IEEE Technical Communities. He is also an Active Reviewer Member of various international journals and conferences, including IEEE and IET. He was a recipient of IEEE Access award "Reviewer of Month," in 2019, for his valuable and thorough feedback on manuscripts. He was a recipient of the Best Paper cum Most Excellence Research Paper Award from the IET-CEAT, in 2016, the IEEE-ICCPCT, in 2014, and the ETAEERE, in 2016 sponsored lecture note in Electrical Engineering, Springer book series.

MOHAMMAD MERAJ (S'17) received the bachelor's degree in electrical engineering from Osmania University, Hyderabad, India, in 2012, the M.Tech. degree from IIT Kharagpur, India, and the master's degree in electrical engineering from IIT Kharagpur, in 2014. He is currently pursuing the Ph.D. degree in electrical engineering with Qatar University, Qatar. He was with Phillips, Bengaluru, in 2013, and a Research Associate with the Department of Electrical Engineering, Qatar University, from 2014 to 2017. He has published scientific papers in the field of power electronics, with particular reference to multiphase dc/ac converter, dc–dc converter, and renewable energy. His research interests include the areas of power electronics converters, control, and electric drives.

ATIF IQBAL (M'08–SM'11) received the B.Sc. (Hons.) and M.Sc. degrees in engineering (power system and drives) from Aligarh Muslim University (AMU), Aligarh, India, in 1991 and 1996, respectively, and the Ph.D. degree from Liverpool John Moores University, Liverpool, U.K., in 2006. He was a Full Professor of electrical engineering with AMU. He is also an Associate Professor of electrical engineering with Qatar University, Doha, Qatar. He has been a Lecturer with the Department of Electrical Engineering, AMU, Aligarh, since 1991, where he served as a Full Professor, until 2016. He has published widely in international journals and conferences his research findings related to power electronics and renewable energy sources. He has authored/coauthored more than 300 research papers, and one book and three chapters in two other books. He has supervised several large Research and Development projects. His research interests include modeling and simulation of power electronic converters, control of multi-phase motor drives, and renewable energy sources. He became a Fellow of IET, U.K., in 2018, and IE, India, in 2012. He was a recipient of the Outstanding Faculty Merit Award AY (2014–2015) and the Research Excellence Award at Qatar University. He was a recipient of the Maulana Tufail Ahmad Gold Medal for standing first at B.Sc. Engg. Exams from AMU, in 1991. He received the Best Research Paper Awards at the IEEE ICIT-2013, IET-SESICON-2013, and SIGMA 2018. He is also an Associate Editor of the IEEE Transactions on Industry Applications and the Editor-in-Chief of the *Journal of Electrical Engineering* (i-manager).